Supporting information for

DFT-quality adsorption simulations in metal-organic frameworks enabled by machine learning potentials

Ruben Goeminne, Louis Vanduyfhuys, Veronique Van Speybroeck, and Toon Verstraelen*

Center for Molecular Modeling (CMM), Ghent University, Technologiepark 46, 9052 Zwijnaarde, Belgium

E-mail: Toon.Verstraelen@UGent.be

Keywords: adsorption, metal-organic frameworks, machine learning, open-metal sites

S1 Benchmarking of DFT settings

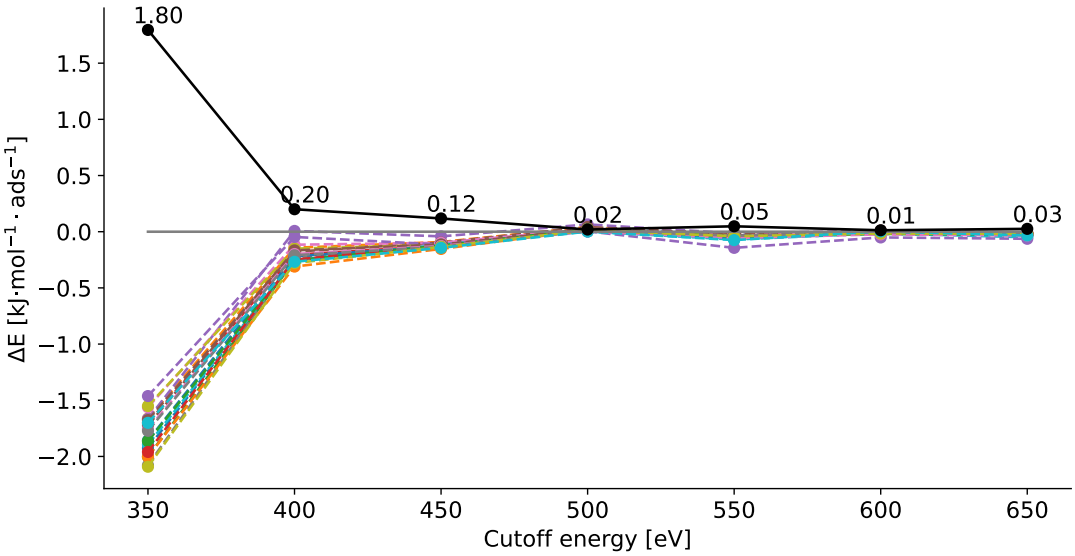

Figure S1: Difference in interaction energy per adsorbate as a function of the cutoff energy compared to the energy at 700 eV for each of the 20 optimized structures. The mean absolute error (MAE) for all 20 structures as a function of the cutoff energy is shown as the black curve.

All single point calculations were performed with VASP, using the projected augmented wavefunction (PAW) PBE potentials.[1–4] The electronic convergence threshold for the energy was set to 10^{-5} eV. For ZIF-8, the PBE-D3(BJ) functional was used with a single k-point. An appropriate value for the cutoff energy for CO_2 adsorption in ZIF-8 was determined by performing 20 optimizations of guest-loaded frameworks for 30 steps using a cutoff of 700 eV. The final 20 structures were recomputed with cutoff energies between 350 eV and 650 eV. The difference between the interaction energies per adsorbate with respect to those at 700 eV are shown in Figure S1. As can be seen, the interaction energy is converged to within 0.05 kJ·mol^{-1} using a cutoff energy of 500 eV, which is the value used in this work. For Mg-MOF-74, a slightly higher cutoff energy of 600 eV was, used in accordance with previous work.[5] The k-point convergence was benchmarked by performing 20 optimizations of the guest-loaded Mg-MOF-74 for 30 steps with each of the three functionals (PBE-D3(BJ), PBE-TS

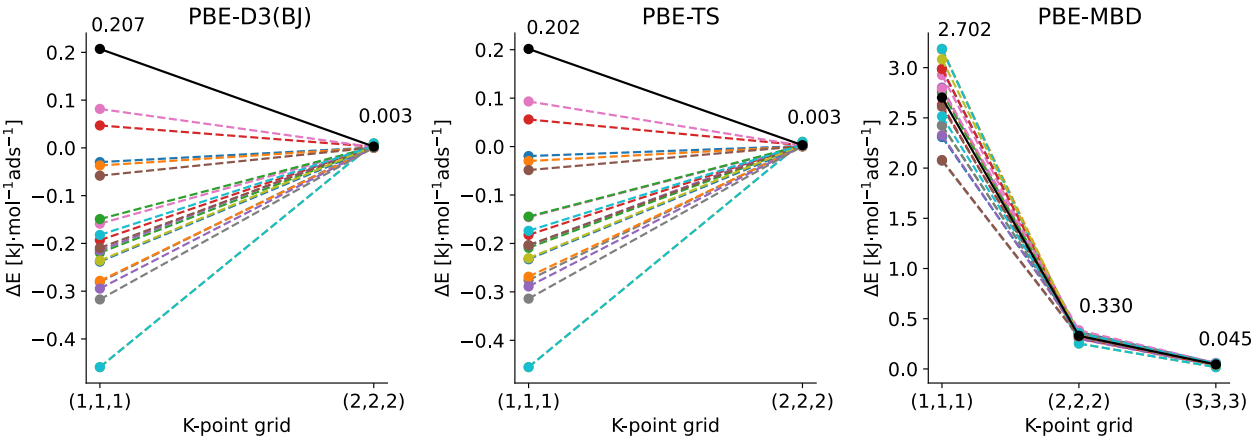

Figure S2: Difference in interaction energy per adsorbate for each of the 20 optimized structures as a function of the k-point grid compared to the a $3 \times 3 \times 3$ grid for PBE-D3(BJ) and PBE-TS, and a $4 \times 4 \times 4$ grid for PBE-MBD. The mean absolute error (MAE) for all 20 structures as a function of the cutoff energy is shown as the black curve.

and PBE-MBD). For the MBD dispersion correction, its reciprocal space implementation can require larger k-point grids than the other methods.[5] Therefore, a $3 \times 3 \times 3$ k-point grid was used for PBE-D3(BJ) and PBE-TS, and a $4 \times 4 \times 4$ k-point grid for PBE-MBD. The final 20 structures of the optimizations were then recomputed with k-point grids between $1 \times 1 \times 1$ and the largest grid used during the optimizations. The resulting difference in interaction energies per adsorbate are shown in Figure S2. From these results a $2 \times 2 \times 2$ k-point mesh was used for all PBE-D3(BJ) and PBE-TS calculations, and a $3 \times 3 \times 3$ k-point mesh for all PBE-MBD calculations. Furthermore, as the difference between calculations performed with the precision set to normal compared to accurate is also within 0.05 kJ·mol^{-1}, the precision was set to normal. For the optimizations, the BFGS optimizer from ASE was used with a maximum step size of 0.5 Å.[6]

S2 Determination of the MLP hyperparameters

The most important properties of the MLPs for use in GCMC calculations is their accuracy and computational efficiency. Therefore, the effect of different hyperparameters of the network on both properties are tested. This is achieved by considering a 'reference' set of

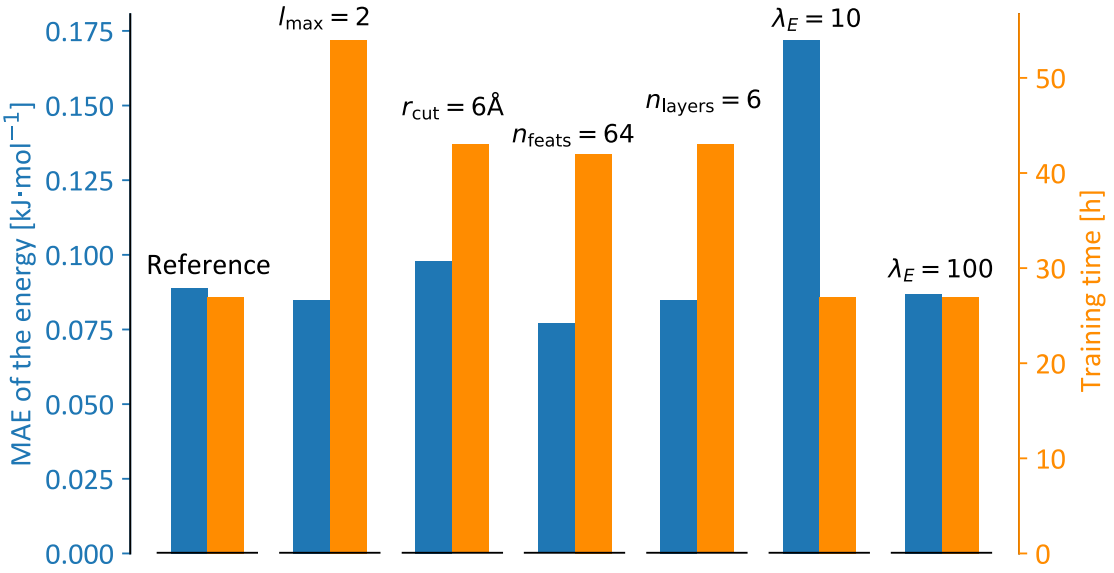

Figure S3: The MAE on the energy per adsorbate and training time to complete 150 epochs for the reference set of hyperparameters, and for sets modifying one of the hyperparameters with respect to the reference set.

hyperparameters and modifying one at a time. The reference parameters are as follows: a cutoff radius $r_{\text{cut}} = 5$Å is used, combined with 4 interaction layers ($n_{\text{layers}} = 4$), 32 features ($n_{\text{feats}} = 32$), a maximum rotation order of 1 ($l_{\text{max}} = 1$) and weights for the energies and forces respectively equal to $\lambda_E = 50$ and $\lambda_F = 1$. In Figure S3, the validation MAE of the energy per adsorbate and the required time for training (for 150 epochs) for the reference hyperparameters are shown on the leftmost blue and orange bars. The same properties for MLPs trained with modified hyperparameters are shown by the other sets of bars. As can be seen, increasing the computational cost by increasing l_{max} to 2, n_{feats} to 64 or n_{layers} to 6 does not significantly decrease the MAE on the energy. Increasing r_{cut} to 6Å even slightly increases the error. Increasing the weight of the energies λ_E to 100 also does not decrease the MAE on the energy, although decreasing it to 10 increases the error significantly. Therefore, the reference set of hyperparameters are used in the remainder of this work.

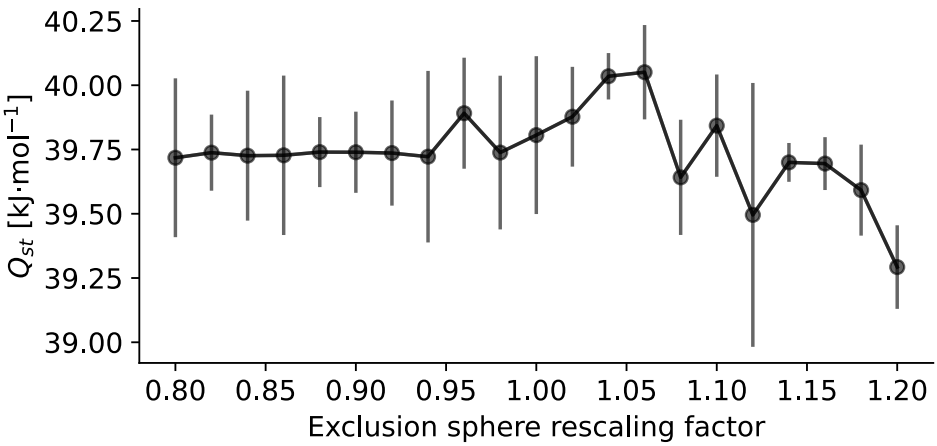

Figure S4: Isosteric heat of adsorption Q_{st} of CO_2 in Mg-MOF-74 obtained from $5 \cdot 10^6$ Widom insertions with rescaled exclusion sphere radii. Errors are obtained from dividing the set of $5 \cdot 10^6$ Widom insertions in 5 subsets, and computing the standard deviation between Q_{st} obtained for each subset.

S3 Validation of the open-metal exclusion radius in Mg-MOF-74

To allow insertions of CO_2 molecules close to the Mg open-metal site in Mg-MOF-74, the Mg van der Waals radius used in the definition of the exclusion radii was set to 1.0 Å. To ensure that this choice does not affect the obtained results, the heats of adsorption Q_{st} at 298 K of CO_2 in Mg-MOF-74 were computed by means of Widom insertions with rescaled values for the radii of the exclusion spheres, with a factor between 0.80 and 1.20. To demonstrate that the region excluded by the exclusion spheres is an irrelevant part of the phase space, the obtained heats of adsorption should be the same with rescaling factors of the exclusion radii smaller than 1. As shown in Figure S4, this is indeed the case. Only at significantly larger exclusion radii (rescaled with a factor 1.2) do the obtained heats of adsorption deviate.

S4 Availability of simulation data

A zip file containing the simulation data and software implementations is archived on Zenodo (10.5281/zenodo.7904959).

References

(1) Kresse, G.; Hafner, J. Ab initio molecular dynamics for liquid metals. *Physical Review B* **1993**, *47*, 558–561.

(2) Kresse, G.; Furthmüller, J. Efficient iterative schemes for ab initio total-energy calculations using a plane-wave basis set. *Physical Review B - Condensed Matter and Materials Physics* **1996**, *54*, 11169–11186.

(3) Kresse, G.; Furthmüller, J. Efficiency of ab-initio total energy calculations for metals and semiconductors using a plane-wave basis set. *Computational Materials Science* **1996**, *6*, 15–50.

(4) Joubert, D. From ultrasoft pseudopotentials to the projector augmented-wave method. *Physical Review B - Condensed Matter and Materials Physics* **1999**, *59*, 1758–1775.

(5) Rehak, F. R.; Piccini, G.; Alessio, M.; Sauer, J. Including dispersion in density functional theory for adsorption on flat oxide surfaces, in metal-organic frameworks and in acidic zeolites. *Physical Chemistry Chemical Physics* **2020**, *22*, 7577–7585.

(6) Hjorth Larsen, A.; JØrgen Mortensen, J.; Blomqvist, J.; Castelli, I. E.; Christensen, R.; Dułak, M.; Friis, J.; Groves, M. N.; Hammer, B.; Hargus, C.; Hermes, E. D.; Jennings, P. C.; Bjerre Jensen, P.; Kermode, J.; Kitchin, J. R.; Leonhard Kolsbjerg, E.; Kubal, J.; Kaasbjerg, K.; Lysgaard, S.; Bergmann Maronsson, J.; Maxson, T.; Olsen, T.; Pastewka, L.; Peterson, A.; Rostgaard, C.; SchiØtz, J.; Schütt, O.; Strange, M.; Thygesen, K. S.; Vegge, T.; Vilhelmsen, L.; Walter, M.; Zeng, Z.; Jacobsen, K. W. The atomic simulation environment - A Python library for working with atoms. *Journal of Physics Condensed Matter* **2017**, *29*, 30.